NUKLEONIKA 2025;70(2):43–49
doi: 10.2478/nuka-2025-0005

TECHNICAL NOTE

sciendo

Effects of irradiating the beam dump with the main electron beam of the superconducting linear accelerator PolFEL

Adam Wasilewski

Abstract. The transport of both primary and secondary radiation in the beam dump was conducted using Monte Carlo analysis. The radiation leakage level through the shielding walls of the bunker of the superconducting, linear electron accelerator PolFEL during beam operation, as well as the radiation dose generated by radioactivity, and the activity level of the beam dump and soil after beam operation were examined. The analysis encompassed three main electron beams with energies of 72 MeV, 187 MeV, and 280 MeV, corresponding to the need to deposit in the beam dump 900.0 W, 935.1 W, and 1400.1 W of electron beam power, respectively. It was determined that 99.86%, 99.83%, and 99.81% of the primary electron beam power was deposited in the designed beam dump. It was determined that the radiation leakage level through the lateral walls of the bunker, outside which nonexposed workers may stay, should be $<1.8 \cdot 10^{-4}$ μSv/h, 0.008(5) μSv/h, and 0.10(2) μSv/h, respectively. It was calculated that the radiation dose rate generated by radioactivity allows staying on the shielding plates above the beam dump no earlier than about a day after the end of the 30 days exposure period of the beam dump. The maximum activity level for the soil activity level at the most exposed location should be <0.008 Bq, 3.37(15) Bq, and 29.8(9) Bq for indicated above electron beam energies, respectively.

Keywords: FLUKA • Monte Carlo calculations • PolFEL linear electron accelerator • radiation shielding

Introduction

Electron accelerators should be equipped with a device design to capture the used and no longer needed electron beam. Typically, such a device is a beam dump, which disperses the concentrated energy of the electron beam and converts it into secondary radiation, with photon and neutron radiation being the most challenging to shield. This study focuses on Monte Carlo calculations of the effects of such radiation and the quality of the shielding used, in particular, to assure that the designed shielding is adequate.

The linear superconducting electron accelerator PolFEL being developed at the National Centre for Nuclear Research [1–4] is planned to be equipped with a single beam dump located at the end of the electron beam transport line. It is envisaged that the beam dump will receive beams with energies of 72 MeV, 187 MeV, or 280 MeV, with an average beam current of 12.5 μA for the lowest of energy, or 5 μA for two higher energies, corresponding to the need to deposit 900.0 W, 935.1 W, or 1400.1 W of electron beam power, respectively.

A. Wasilewski
National Centre for Nuclear Research
Andrzeja Sołtana St. 7, 05-400 Otwock-Świerk, Poland
E-mail: Adam.Wasilewski@ncbj.gov.pl

Received: 18 April 2024
Accepted: 12 November 2024

The beam dump for the superconducting linear electron accelerator PolFEL has been designed based on a project developed for a similar device located at the XFEL accelerator [5, 6]. However, for the PolFEL accelerator project, it was proposed that the core of the beam dump was made of aluminum instead of graphite due to its better material properties. Additionally, to reduce the intensity of radiation emitted from the entire beam dump system, it was decided to add an additional steel shield around the standard copper layer surrounding the aluminum core.

Other Monte Carlo calculations for beam dumps can be found in Refs. [7–9].

Computational methods

While modeling the bunker geometry for Monte Carlo calculations, efforts were made to accurately replicate the actual design of the planned bunker and most of the equipment that had the greatest potential for significant influence on the generated radiation. The geometry of the entire bunker of the PolFEL accelerator is shown in Fig. 1. It was assumed that walls (S) and (N), made of Portland concrete, are to have a thickness of 2 m. To the north of wall (N), additional shielding is provided by the walls of the existing proton accelerator hall, with thickness ranging from 40 cm to 70 cm depending on the location. The thicknesses of the other barite concrete walls are as follows: wall (NW) is 1.5 m, wall (D) is 2 m, walls (A) and (C) are 2.5 m, and walls (B) and (E) are 3 m. It was further assumed that both the floor and the roof of Portland concrete are to be 2 m thick, but that part of the roof over the beam dump requiring better shielding, as shown in Fig. 2, have to be of barite concrete. The main entrance (en) is closed with shielding doors of typical construction, consisting of 1-cm stainless steel, 27-cm paraffin, 3-cm lead, and 1-cm stainless steel, from the accelerator hall. For computational purposes, the entire bunker of the PolFEL accelerator was placed on a layer of soil, 5.5 m thick. The chemical composition of selected concretes and soil used in the calculations is presented in Table 1.

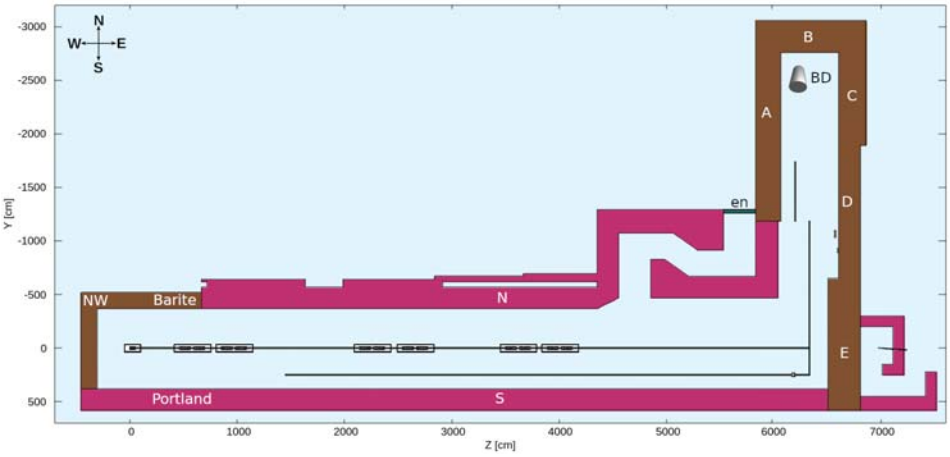

Fig. 1. The horizontal cross section of the entire bunker for the PolFEL accelerator with the marked location, where the beam dump is positioned below the floor level (BD). A view of the layout for a beam energy of 280 MeV at the beam axis level. There are two less accelerating cryomodules for calculations with 72 MeV and 187 MeV beam energy than with the highest one. One can see the second beam pipe of the THz line, parallel to the beam pipe for VUV line in a distance of 2.5 m to the south. Side walls A, B, C, D, E, and NW are of barite concrete, and the other walls are of Portland concrete.

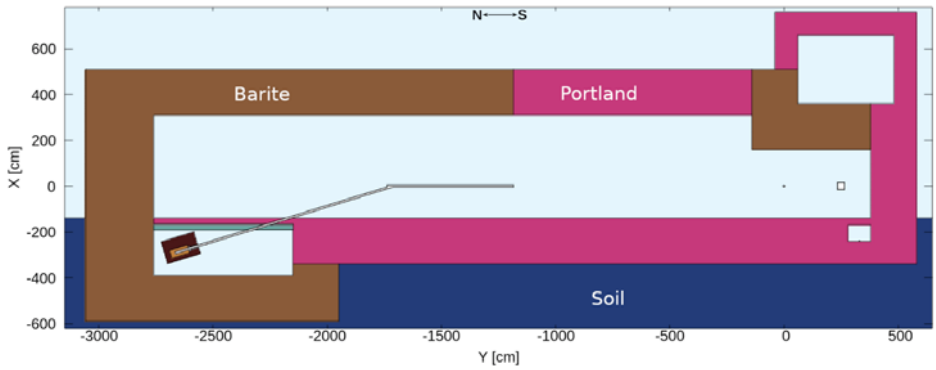

Fig. 2. Vertical N-S section through the whole bunker branch with the dump room along the beam dump axis. The dump room is covered with three plates, 20-cm polyethylene, 5-cm aluminum, and 25-cm concrete Portland, counting from below. One can see a steel beam pipe with an inner diameter of 7.8 cm and a SS316LN wall thickness of 3 mm, sloping at an angle of 17°, leading to the beam dump. The dump room is shielded from below by a floor with a thickness of 2 m of barite concrete. Additionally, the floor of the bunker branch made of Portland concrete with a thickness of 2 m can be seen, terminating at the ground level. The ceiling of the entire bunker is 2 m thick, regardless of the planned material to be used.

Table 1. Density and chemical composition of materials used for calculations. Chemical composition in terms of weight

Density (g/cm³)	Portland concrete 2.3	Barite concrete 3.2	SS316LN 7.8	Soil 2.7
H (Z = 1)	2.2%	0.4%	–	–
C (Z = 6)	0.3%	–	0.03%	
O (Z = 8)	57.1%	31.2%	–	47%
Na (Z = 11)	1.5%	–	–	3%
Mg (Z = 12)	0.1%	0.1%	–	2%
Al (Z = 13)	2.1%	0.4%	–	8%
Si (Z = 14)	30.6%	1.0%	1.00%	28%
P (Z = 15)	–	–	0.05%	–
S (Z = 16)	–	10.8%	0.03%	–
K (Z = 19)	1.1%	–	–	3%
Ca (Z = 20)	4.3%	5.0%	–	4%
Cr (Z = 24)	–	–	18.50%	–
Mn (Z = 25)	–	–	2.00%	–
Fe (Z = 26)	0.7%	4.8%	67.14%	5%
Ni (Z = 28)	–	–	11.25%	–
Ba (Z = 56)	–	46.3%		

The beam dump is placed in a special room, situated below the ground level, designed to provide optimal shielding for the beam dump both during beam operation and after its shutdown. The geometry of the beam dump room with the installed beam dump and the geometry of the bunker branch are shown in Figs. 2 and 3, respectively. For the purpose of the room that will house the beam dump, an excavation in the ground with a depth of 4.5 m and dimensions of 11.1 m × 10.3 m horizontally is planned, while the dimensions of the dump room itself are planned to be 6.1 m × 2.8 m horizontally with a height of 2 m. On the north and west sides, the dump room is shielded with a 3-m thick wall made of barium concrete, while on the east side with a thickness of 2.5 m, the dump room is covered from the top with three removable layers of plates with horizontal dimensions, a 20-cm thick polyethylene layer, a 5-cm

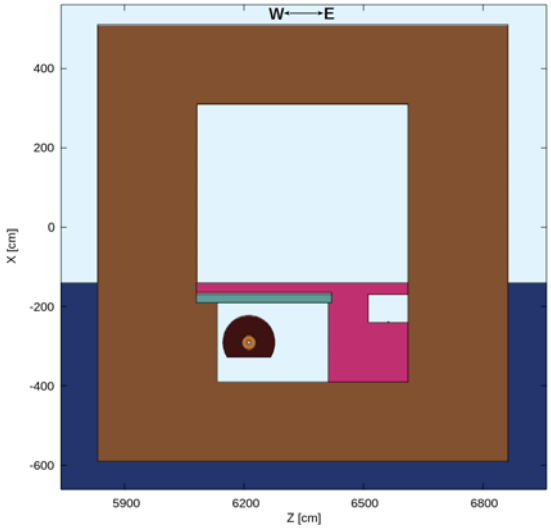

Fig. 3. Vertical E-W section through the beam dump and the dump room. One can see the side walls and ceiling of the bunker branch made of barite concrete and the level of the ground surface.

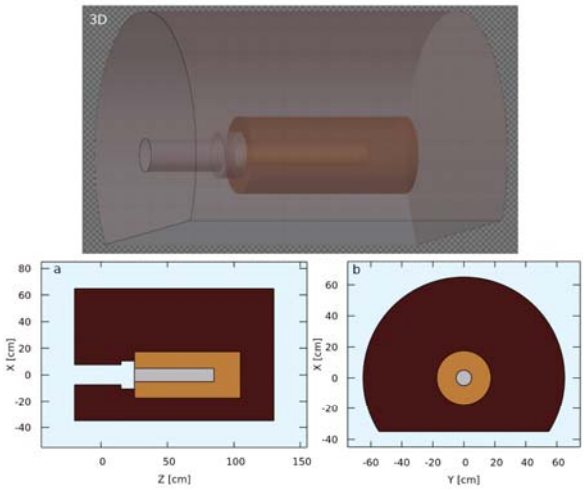

Fig. 4. Geometry used for Monte Carlo calculations of the radiation transport generated in the beam dump. A cross section parallel to beam axis through the dump (A), a cross section perpendicular to beam axis (B), and 3D view of the beam dump are shown. One can see 10-cm diameter and 60-cm high Al core, surrounded by a 35-cm diameter and 80-cm high copper layer and a 130-cm diameter and 150-cm high SS316LN steel layer.

thick aluminum layer, and a 25-cm thick concrete layer, counting from the side of the dump room. The beam dump is positioned so that its axis aligns with the axis of the electron beam pipe after bending downward at an angle of 17°. The roof of the bunker directly above the dump room is made of 2-m thick barite concrete.

The geometry of the beam dump is shown in Fig. 4. The beam dump is designed as an aluminum cylinder with a height of 60 cm and a diameter of 10 cm, which is placed inside a copper cylinder with a height of 80 cm and a diameter of 35 cm, which is placed inside a cylinder with a height of 150 cm and a diameter of 130 cm made of SS316LN steel. All these cylinders are coaxial. The outer steel cylinder from the bottom side has a cutout located 35 cm away from the common axis of all cylinders. In the steel shield on the side of electron beam delivery, two cylindrical recesses were designed, one closer to the aluminum core with a height of 10 cm and a diameter of 21 cm and the other further with a height of 35 cm and a diameter of 15 cm. It is planned that the electron beam will be delivered to the beam dump through a vacuum tube with an internal diameter of 7.8 cm made of SS316LN steel with a thickness of 3 mm. The chemical composition of the SS316LN steel used in the calculations is presented in Table 1.

The Monte Carlo calculations were conducted using the FLUKA code 2020 [10, 11] installed on the computing cluster at the Świerk Computing Centre (CIŚ) [12], operated by the National Centre for Nuclear Research. In these calculations, an electron beam with full width at half maximum (FWHM) of 2 mm and a spatial divergence of 0.1 mrad was used. The beam was positioned 40 cm away from the exposed surface of the aluminum core within the beam dump. The calculations were performed for monoenergetic beams, with the assumption that the real beams will not exceed these energies. This

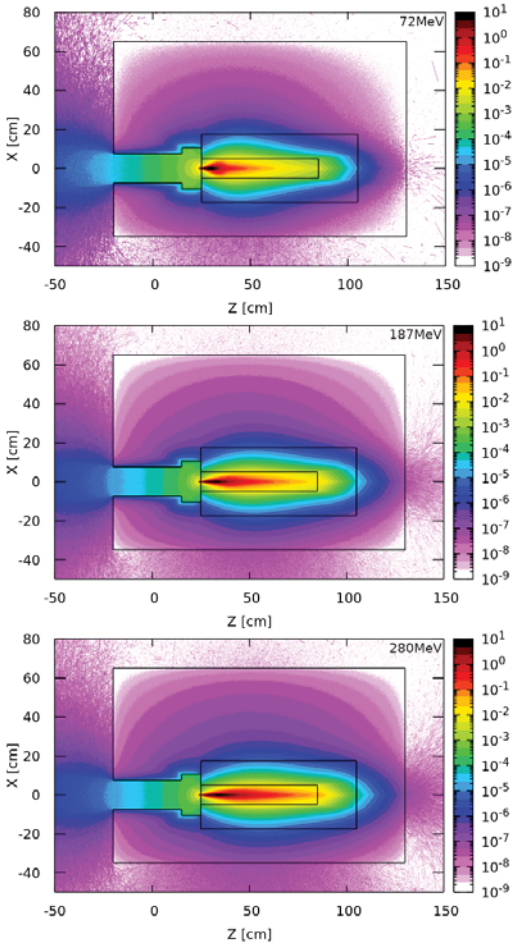

Fig. 5. The dose rate deposited in the beam dump by beams with energies 72 MeV, 187 MeV, and 280 MeV. The quantities shown in W/g.

is an assumption that the actual beams will generate a lower dose rate of secondary radiation compared to monoenergetic beams, which is beneficial from a radiological protection perspective. Transport cutoffs were set at 100 keV for electrons, 30 keV for photons, and 10^{-5} eV for neutrons. It was assumed that the electron beam would operate continuously for 30 days.

Results and discussion

The spatial distribution of the dose rate and the dose rate generated in the beam dump obtained as a result of calculations are shown in Fig. 5. According to the calculations, the power of 782.2 W, 784.7 W, and 1161.6 W would be deposited in the aluminum cylinder, at the assumed currents and energies. The power of 898.8 W, 933.5 W, and 1397.5 W would be deposited in the entire beam dump, which is 99.86%, 99.83%, and 99.81% of the power of the primary electron beam, respectively. From the perspective of radiation protection, three main physical processes occur in the beam dump. Electrons interacting with the aluminum core of the dump generate bremsstrahlung radiation; the lower the atomic number (Z) of the core material, the less bremsstrahlung is produced. The resulting photon bremsstrahlung is attenuated by Compton scattering

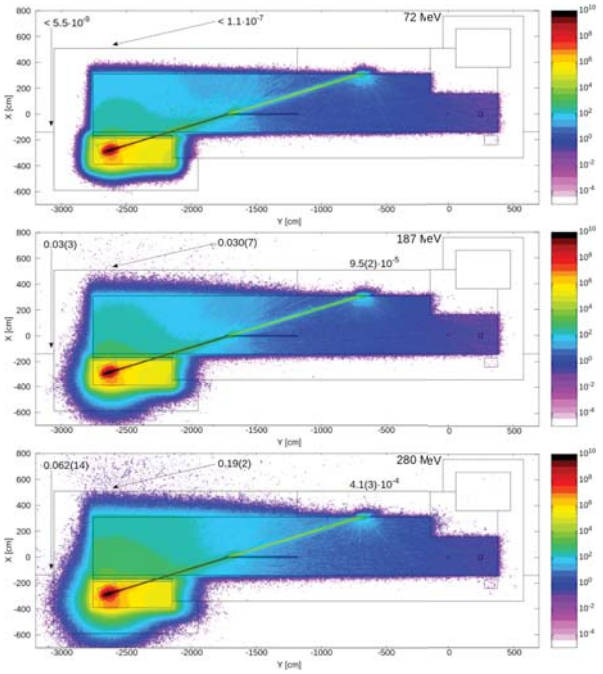

Fig. 6. Distribution of the radiation dose rate in μSv/h in the vertical plane parallel to the beam axis for the 72-MeV, 187-MeV, and 280-MeV beams.

and electron–positron pair production within both the inner copper and outer steel layers of the dump covers. However, since a portion of the photons have energies exceeding the neutron separation energy in the materials of the dump cover layers, photonuclear reactions leading to neutron emission may occur.

The level of radiation leakages outside the walls of the bunker branch was determined based on the dose rate calculated directly outside these walls. The results of radiation transport calculations generated in the irradiated beam dump within the bunker branch are presented in Figs. 6 and 7. The results of radiation leakage calculations through the external walls of the bunker for beams of 187 MeV and 280 MeV are presented in Table 2. It can be observed that in almost all accessible areas, the radiation level outside the external walls of the bunker does not exceed the assumed safety level of 0.15 μSv/h [13–15]. The exception is the roof of the bunker branch directly above the beam dump irradiated with the 280 MeV beam, where the radiation dose rate is 0.19 μSv/h. However, it should be noted that this is

Table 2. Summary of the radiation leaks outside the bunker branch walls calculated directly for 187 MeV and 280 MeV and estimated on the basis of the dose rate attenuation in the branch walls shown in Fig. 8 for 72 MeV. Radiation leakages through walls D and E are so small that it has not been possible to estimate their magnitude

Place	72 MeV	187 MeV	280 MeV
	Total dose rate (μSv/h)		
A	$<1.8 \times 10^{-4}$	0.008(5)	0.10(2)
B	$<5.5 \times 10^{-9}$	0.030(3)	0.062(14)
C	$<6.0 \times 10^{-11}$	0.005(2)	0.016(4)
D and E	–	0.005(2)	0.019(6)
Roof	$<1.1 \times 10^{-7}$	0.030(7)	0.19(2)

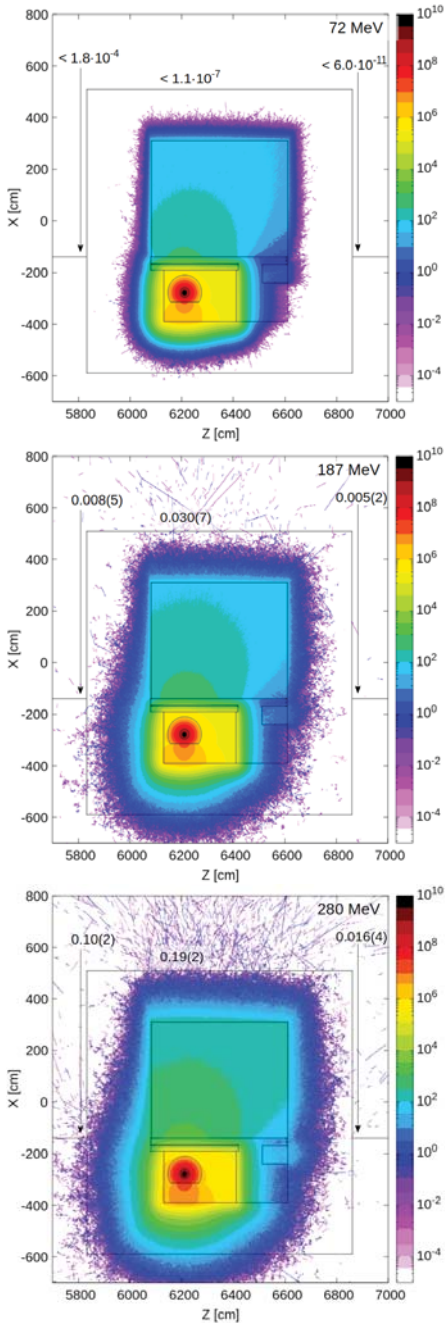

Fig. 7. Distribution of the radiation dose rate in μSv/h in the vertical plane perpendicular to the beam axis for the 72-MeV, 187-MeV, and 280-MeV beams.

a difficult-to-access area, so it can be assumed that no one will stay in this place for too long, especially during beam operation.

Due to the intense absorption of secondary radiation generated by the 72-MeV beam in the walls of the bunker branch, it was not possible to obtain radiation leakage results outside using direct calculations. Given the observation that the radiation level outside is at least 12 orders of magnitude lower than the dose rate in the area of the aluminum core of the beam dump, a method assuming exponential decay of the radiation dose rate in the shielding walls of the bunker branch and possible extrapolation of the dose rate level beyond the walls was applied. This extrapolation is presented in Fig. 8. As a result, an

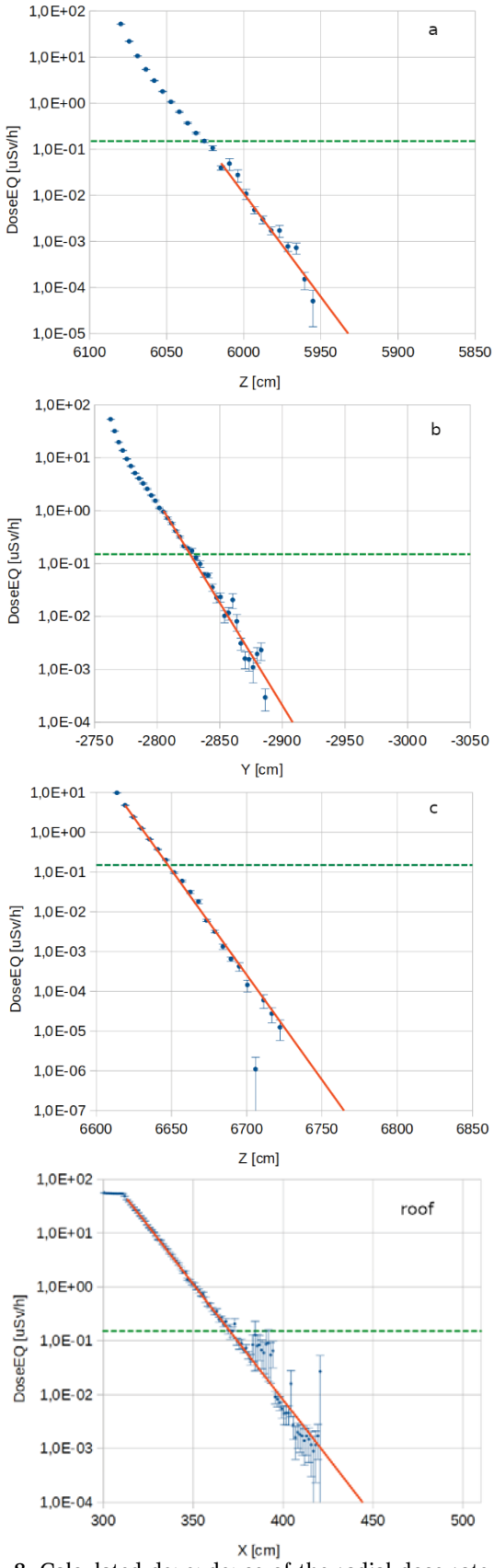

Fig. 8. Calculated dependence of the radial dose rate depending on the location. Exponential decay of the dose rate was fitted to the data calculated directly from Monte Carlo calculations. The right end of each of the graphs presented here indicates the outer end of the respective shielding wall. Figures (a–c) show the decay of the deposited dose rate in walls A–C, respectively.

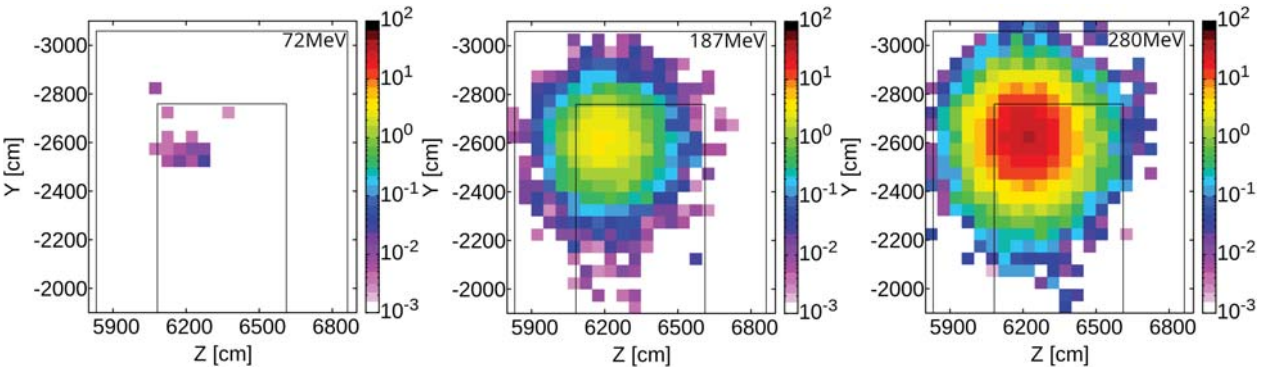

Fig. 9. The distribution of activation generated in a 50-cm thick soil layer directly below the dump room shown against the walls of the bunker branch. The soil activation levels in Bq/cm^3 for electron beams with energies of 72 MeV, 187 MeV, and 280 MeV are shown.

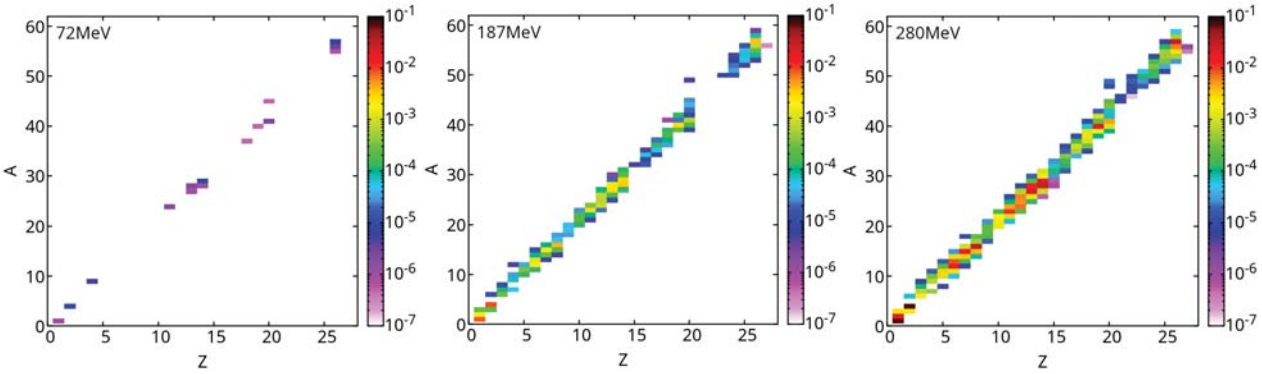

Fig. 10. The residual nuclei produced on-beam in the soil region directly below the beam dump room for the 72-MeV, 187-MeV, and 280-MeV beams. The data presented in the figures are expressed in nuclei/cm^3/s.

upper estimate of the radiation leakages through the shielding walls of the branch for the 72-MeV beam is obtained, as shown in Table 2.

The radiation generated within the beam dump during irradiation will penetrate through a barite concrete floor with a thickness of 2 m. Despite such thick shielding, some radiation will penetrate into the soil, triggering its activation. The maximum values of average soil activation directly beneath the dump room are shown in Table 3, while the distribution of soil activation is shown in Fig. 9. The phenomenon of soil activation is primarily caused by photonuclear reactions occurring within the soil itself, as well as the capture of neutrons that have already been generated. As a consequence of these reactions, the resulting nuclei are typically not situated on the beta decay stability path, which makes them radioactive. The isotopes that are formed in the soil as a consequence of the aforementioned reactions are illustrated in Fig. 10.

Table 3. Summary of the maximum soil activity averaged in 50 cm × 50 cm × 50 cm cubes directly below the dump room

Cooling time	72 MeV	187 MeV	280 MeV
	Maximum activity from the beam (Bq/cm^3)		
1 min	$<8 \times 10^{-6}$	$3.37(15) \times 10^{-3}$	$2.98(9) \times 10^{-2}$
1 h	$<8 \times 10^{-6}$	$1.55(8) \times 10^{-3}$	$1.36(5) \times 10^{-2}$
1 day	$<8 \times 10^{-7}$	$5.3(3) \times 10^{-4}$	$4.7(2) \times 10^{-3}$
1 week	$<8 \times 10^{-7}$	$9.6(19) \times 10^{-5}$	$8.5(12) \times 10^{-4}$
30 days	$<8 \times 10^{-7}$	$6.9(13) \times 10^{-5}$	$6.0(8) \times 10^{-4}$
1 year	$<2 \times 10^{-7}$	$1.1(2) \times 10^{-5}$	$9.9(9) \times 10^{-5}$

Conclusion

During the operation of each of the designed electron beams with energies of 72 MeV, 187 MeV, and 280 MeV, both the beam dump and the walls of the bunker branch ensure that the level of secondary radiation outside the bunker is sufficiently low to be considered safe.

The secondary radiation generated in the beam dump during accelerator operation will only generate minor radioactivity in the soil, which should not exceed a maximum level of ~0.03 Bq/cm^3, which corresponds ~30 Bq/l.

Acknowledgments. The PolFEL project was supported by the European Regional Development Fund in the framework of the Smart Growth Operational Programme, Measure 4.2: Development of modern research infrastructure of the science sector.

ORCID

A. Wasilewski https://orcid.org/0000-0002-2109-5833

References

1. Romaniuk, R. S. (2009). POLFEL – A free electron laser in Poland. *Photonics Letters of Poland, 1*(3), 103–105. DOI: 10.4302/plp.2009.3.01.
2. Sekutowicz, J., Czuma, P., Krawczyk, P., Kurek, K., Lorkiewicz, J., Nietubyć, R., Poliński, J., Staszczak, M., Szamota-Leandersson, K., & Szewiński, J. (2019). Polish free electron laser: short technical description. *Proceedings of SPIE*, *11054*, 1105405. DOI: 10.1117/12.2526756.
3. Szamota-Leandersson, K., Nietubyć, R., Czuma, P., Krawczyk, P., Krzywiński, J., Sekutowicz, J., Staszczak, M., Szewiński, J., Bal, W., Poznański, J., Bartnik, A., Fiedorowicz, H., Janulewicz, K., & Pałka, N. (2019). PolFEL – New facility in Poland. In 39th Free-Electron Laser Conference, 26–30 August 2019 (pp. 746–748). Hamburg, Germany: JACoW Publishing. DOI: 10.18429/JACoW-FEL2019-THP081.
4. Nietubyć, R., Banaszkiewicz, T., Bartnik, A., Chorowski, M., Czuma, P., Duda, P., Grabowski, W., Horodeński, A., Fiedorowicz, H., Felisiak, P., Fok, T., Janulewicz, K., Kopeć, J., Kowalski, G., Krawczyk, P., Krzywiński, J., Kwiatkowski, R., Lorkiewicz, J., Nowak, M., Michalski, G., Marendziak, A., Matusiak, M., Pałka, N., Panaś, R., Poliński, J., Romanowicz, P., Sekutowicz, J., Sosnowski, J., Staszczak, M., Szamota-Leandesson, K., Szewiński, J., Tazbir, J., Terka, M., Wawrzyniak, A., Wasilewski, A., Węgrzyński, Ł., Wiechecki, J., Wójtowicz, M., Zagrajek, P., & Ziemiański, D. (2021). Status of PolFEL Project. In 2021 International Conference on Radio Frequency Superconductivity (SRF 21), 28 June–2 July 2021, Tsukuba, Japan. https://indico.frib.msu.edu/event/38/attachments/158/1069/THPFAV003.pdf.
5. Maslov, M., Schmitz, M., & Sychev, V. (2006). *Layout considerations on the 25 GeV/300 kW beam dump of the XFEL Project*. Hamburg: DESY. (TESLA-FEL 2006-05).
6. Altarelli, M., Brinkmann, R., Chergui, M., Decking, W., Dobson, B., Düsterer, S., Grübel, G., Graeff, W., Graafsma, H., Hajdu, J., Marangos, J., Pflüger, J., Redlin, H., Riley, D., Robinson, I., Rossbach, J., Schwarz, A., Tiedtke, K., Tschentscher, T., Vartaniants, I., Wabnitz, H., Weise, H., Wichmann, R., Witte, K., Wolf, A., Wulff, M., & Yurkov, M. (2007). *The European X-Ray Free-Electron Laser. Technical design report*. Hamburg: DESY. (DESY 2006-097).
7. Shi, T., Sun, D., Jovanovic, I., Kalinchenko, G., Krushelnick, K., Kuranz, C. C., Maksimchuk, A., Nees, J., Thomas, A. G. R., & Willingale, L. (2021). Optimization of the electron beam dump for a GeV-class laser electron accelerator. *Appl. Radiat. Isot.*, *176*, 109853. DOI: 10.1016/j.apradiso.2021.109853.
8. Chatterjee, S., Banerjee, K., Pratap, Roy, Bandyopadhyay, T., Bhattacharya, C., & Bhattacharya, S. (2013). Monte Carlo calculations for beam dump shield design for K-130 cyclotron at VECC. *Proceedings on the DAE Symp. Nucl. Phys.*, *58*, 886. http://www.sympnp.org/proceedings/58/G21.pdf.
9. Huang, L., Dejun, E., Tao, K., & Liu, C. (2024). Simulation study of coupled particle cascade and finite element analysis for beam dump of DALS. *Radiation Detection Technology and Methods*, *8*(2), 1254–1263. DOI: 10.1007/s41605-023-00444-7.
10. Böhlen, T. T., Cerutti, F., Chin, M. P. W., Fassò, A., Ferrari, A., Ortega, P. G., Mairani, A., Sala, P. R., Smirnov, G., & Vlachoudis, V. (2014). The FLUKA code: Developments and challenges for high energy and medical applications. *Nucl. Data Sheets*, *120*, 211–214.
11. Ferrari, A., Sala, P. R., Fassò, A., & Ranft, J. (2005). *FLUKA: a multi-particle transport code*. Geneva: CERN. (CERN-2005-10, INFN/TC_05/11, SLAC-R-773).
12. Centrum Informatyczne Świerk. (n.d.). https://www.cis.gov.pl.
13. Council of Ministers of the Republic of Poland. (2006). *Regulation of the Council of Ministers of the Republic of Poland of July 12, 2006, Chapter 2, § 5*. (In Polish).
14. International Atomic Energy Agency. (2006). *Radiation protection in the design of radiotherapy facilities.* Vienna: IAEA. (Safety Reports Series no. 47).
15. International Atomic Energy Agency. (2018). *Radiation protection and safety in medical uses of ionizing radiation*. Vienna: IAEA. (Safety Standards Series no. SSG-46).